Effect of processing parameters on the microstructure and mechanical properties of Al–steel composite foam

L. J. Vendra · J. A. Brown · A. Rabiei

Abstract Al–steel composite foams comprise of steel hollow spheres embedded in an aluminum matrix and are processed using a gravity casting technique. The effect of processing parameters such as casting temperature and cooling rate on the microstructure and mechanical behavior was studied to establish structure–property relationships. Results show that the amount and composition of intermetallic phases present in the foam microstructure is directly related to casting temperature and cooling rate. Highest strength and energy absorption were obtained from Al–steel foams with fast solidification rates that minimize the growth of intermetallic phases.

Introduction

Closed cell metal foams are structural materials well known for their high energy absorption capability during deformation under compressive loads. An interesting combination of properties such as low density, high specific strength, and high ductility make them attractive choices for applications in automobile, aerospace, and construction industries [1]. However, the deformation behavior of most closed cell metal foams is dominated by variations in cell wall thickness and cell size along with morphological defects [2]. Composite metal foams belong to a special class of closed cell metal foams that are designed to overcome the non-uniform deformation behavior evident in other metal foams [3–5]. Al–steel composite foams are processed by infiltrating a random loose arrangement of pre-fabricated steel hollow spheres with an aluminum alloy matrix by gravity casting [6, 7]. The microstructure of the Al–steel composite foam and its mechanical behavior under static compression and cyclic loading has been studied previously [7–9], but further investigation is needed to understand the effects of processing parameters on foam properties. This is particularly relevant since alterations in the processing parameters of metal foams are known to affect the mechanical properties such as ductility and energy absorption [10].

The microstructure of the Al–steel composite foam predominantly consists of aluminum, iron, and silicon. The casting process results in several intermetallic phases forming due to inter-diffusion between iron, chromium, and manganese present in the sphere walls and aluminum and silicon in the aluminum matrix. The microstructure and composition of various intermetallic compounds in Al–Fe–Si system have been described extensively in the literature [11, 12], and a total of 10 different Fe–Al–Si ternary intermetallic phases have been reported earlier [13]. The intermetallic phases in the Al–stainless steel composite foam have been identified previously using results from the Al–Fe–Si ternary phase alloy diagram [14] and SEM-EDS analysis to be $Fe_{25}Al_{60}Si_{15}$ forming an intermediate layer at the sphere–matrix interface, plate-shaped Fe_2Al_7Si found near the edges of the interface layer and needle-shaped $FeAl_4Si$ found in the matrix [7]. Some traces of silicon are also found to be precipitated either along the edges of the needle-shaped phases or distributed in the matrix. The results are consistent with those reported by Fragner et al. regarding the intermetallic phases in the Al alloy–steel composite systems [15].

L. J. Vendra · J. A. Brown · A. Rabiei (✉)
Department of Mechanical and Aerospace Engineering, North Carolina State University, 911 Oval Drive, Campus Box 7910, Raleigh, NC 27695-7910, USA
e-mail: arabiei@ncsu.edu

Present Address:
L. J. Vendra
Baker Hughes, Houston, TX 77073, USA

To produce composite metal foam with controlled microstructure and properties, it is necessary to understand the details of the processing parameters and their effect on foam properties. In this study, the casting temperature and cooling rate of Al–steel composite foam are varied, and the subsequent effect on the composite foam's microstructure and its compressive behavior under loading are studied.

Materials processing and characterization

The Al–steel composite foam is produced by a simple gravity casting technique. The sphere material must have a melting temperature significantly higher than the matrix material to prevent thermal deformation of the spheres during the casting process. Consequently, the combination of steel spheres with an aluminum matrix was chosen. The hollow spheres are pre-fabricated by a powder metallurgy process from 316L stainless steel and have outer diameter of 3.7 mm, wall thickness of 0.2 mm, and wall porosity of 7–8% [16]. The matrix material used is aluminum A356 casting alloy (Al–7% Si).

The mold cavity is filled with hollow spheres and pre-heated to the casting temperature in order to prevent the aluminum from freezing prematurely and obstructing flow between the spheres as it rises in the mold. A 3300 series high temperature laboratory furnace from CM Furnaces is used to preheat the mold while simultaneously melting the aluminum in a graphite crucible. The molten aluminum poured into the sprue of the casting mold rises into the mold cavity where it infiltrates the spaces between the hollow spheres to form a solid matrix. Since the liquidus temperature of aluminum A356 is 615 °C [17], casting temperatures of 700 °C and 740 °C were chosen to have about 15% and 20% overheat, respectively. A minimum overheat of 15% is necessary to prevent a premature solidification of the melt before it has a chance to completely fill the mold. It is also known that an optimum overheat can improve the homogeneity and microstructure of the solidified alloy [18].

Two different cooling methods were used to further study the effects of solidification rate on the Al–steel foam properties. After casting, the samples were either allowed to air cool slowly to room temperature or a faster cooling rate was obtained by water cooling. Water cooling of the Al–steel composite foam samples was achieved by placing copper coils filled with cold running water around the mold after casting. The copper coils were placed around the mold in such a way as to ensure uniform cooling of the sample in the mold cavity. After the copper coils were in place, the mold was also further cooled down by water spraying. Three sets of Al–steel composite foam samples were selected for this study: air-cooled samples with casting temperature of 740 °C, air-cooled samples with casting temperature of 700 °C, and water-cooled samples with casting temperature of 700 °C. For the remainder of the article, these samples will simply be referred to as air-cooled 740 °C, air-cooled 700 °C, and water-cooled 700 °C samples.

The microstructure of one sample with each set of processing parameters was studied using scanning electron microscope (SEM) imaging and the phases were chemically characterized to evaluate the nature of the intermetallics formed using energy dispersive spectroscopy (EDS). Image analysis software (Image-J) was used to measure dimensions of features in the microstructure and to evaluate the percentages of intermetallic phases present. Hardness measurements of various phases in the microstructure of each sample were taken using a Buehler Micromet microhardness tester with a diamond indenter and a load of 20 g.

Monotonic compression tests were performed on air-cooled 740 °C samples, air-cooled 700 °C samples, and water-cooled 700 °C samples to study the influence of the processing parameters and resulting microstructure on mechanical behavior of the Al–steel composite foam. The aspect ratio (height to width) for the compression test samples was maintained in the range of 1.4–1.6 and samples contained at least 8–10 spheres per side in order to eliminate surface effects and represent accurate behavior of the bulk foam material. Tests were conducted on an MTS 810 loading machine with a 220 kip load cell at a crosshead speed of 1.25–1.28 mm/min.

Results

Figure 1 shows low magnification SEM images of Al–steel composite foam samples processed at different temperatures and cooled using different techniques. The boxed areas of the images in Fig. 1 are shown at higher magnifications in Fig. 2. As shown in Figs. 1 and 2, all samples exhibit good bonding between the spheres and matrix and contain three different intermetallic phases: an intermediate layer surrounding the sphere-matrix interface, plate-shaped phases located just outside the intermediate layer, and needle-shaped phases distributed throughout the matrix. Figure 3 shows the area percentage of each phase present in the image for composite foams processed with each set of parameters. These values were obtained by comparing the area occupied by each intermetallic phase to the total area excluding the sphere walls and sphere cavities. Data presented in Fig. 3 was obtained by analysis of the low magnification images shown in Fig. 1.

It can be clearly seen that the air-cooled 740 °C sample has the highest percentage of both intermediate layer and
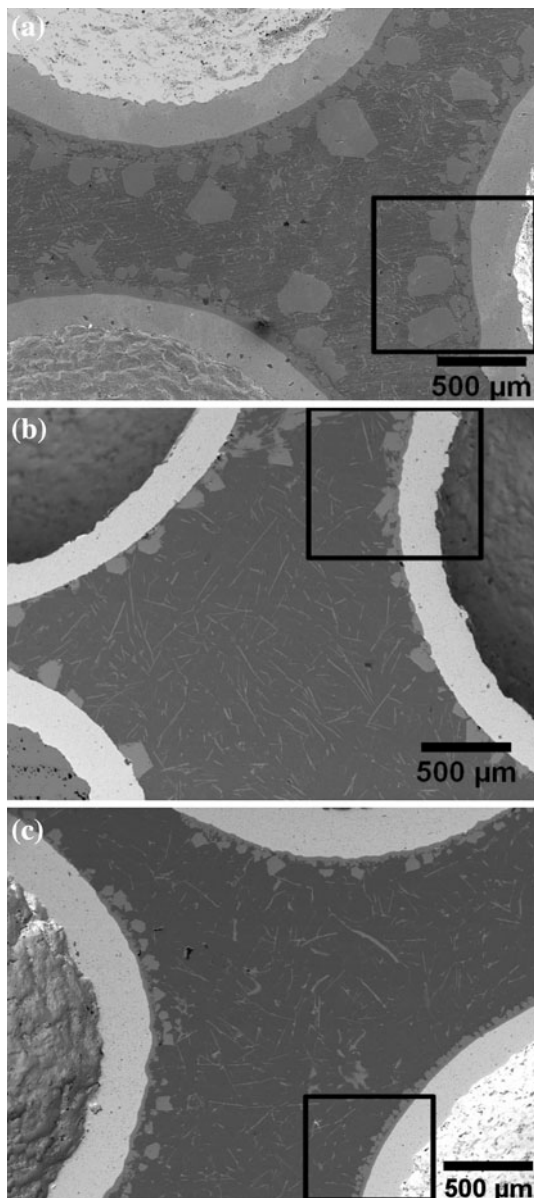
Fig. 1 Low magnification SEM images of CMF showing spheres, matrix, and intermetallic phases for various cooling methods: (a) air-cooled 740 °C, (b) air-cooled 700 °C, (c) water-cooled 700 °C

plate-shaped phases, followed by the air-cooled 700 °C sample, while the water-cooled 700 °C sample has the lowest percentage of these two phases. The percentage of needle-shaped phases is roughly the same between all three sets of processing parameters.

In addition, the thickness of the intermediate layer, size and distribution of the plate-shaped phases, and the morphology of needle-shaped phases are different for each set of processing parameters. Average values of the intermediate layer thickness are 76.9 μm ± 15.7 μm for the air-cooled 740 °C sample, 34.3 μm ± 10.4 μm for the

air-cooled 700 °C sample, and 25.2 μm ± 4.3 μm for the water-cooled 700 °C sample.

In the low magnification image of the air-cooled 740 °C sample (Fig. 1a), there were 48 individual plate-shaped sections with the most common area values falling between 6,000 and 20,000 μm^2. In addition, there were some plate-shaped sections in this sample with smaller areas and several with much larger areas up to 85,000 μm^2. The air-cooled 700 °C sample image (Fig. 1b) had 24 plate-shaped sections with areas mostly falling between 6,000 and 20,000 μm^2. However, unlike the air-cooled 740 °C sample, there were only 2 plate-shaped sections with areas outside this range and none with area greater than 37,000 μm^2. The water-cooled 700 °C sample image (Fig. 1c) had 59 individual plate-shaped sections with areas mostly falling below 3,000 μm^2. None of the plate-shaped sections in the water-cooled 700 °C sample had areas greater than 10,000 μm^2.
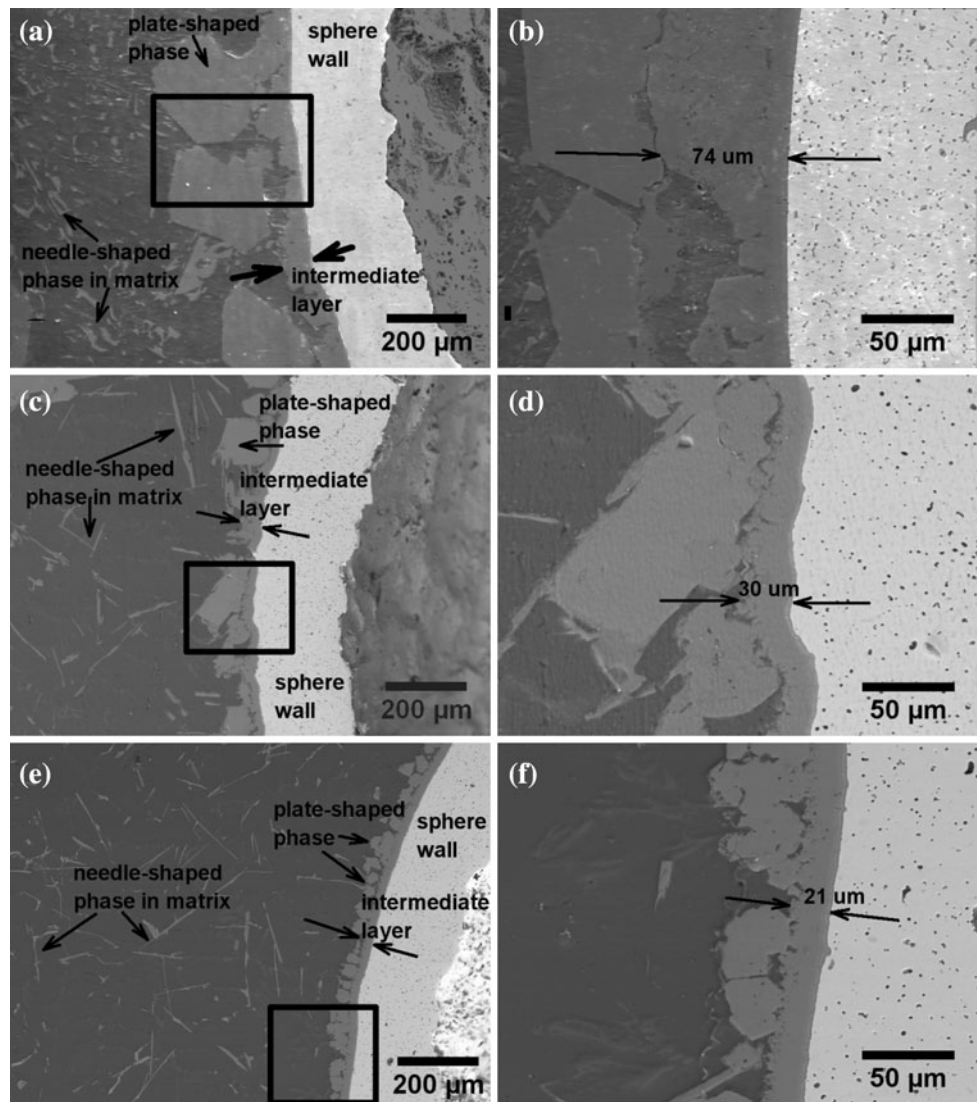
Morphology of the needle-shaped phase for samples from each set of processing parameters is shown in Fig. 4. As shown in the figure, needle-shaped phases in the air-cooled 740 °C sample have very discontinuous, segmented shapes, while this phase in the air-cooled 700 °C sample is much straighter and more uniform. In the water-cooled 700 °C sample, the needle-shaped phase exhibits a more branched structure.

Composition of the various intermetallic phases for each set of sample processing parameters is shown in Table 1. These phases are composed largely of aluminum, iron, and silicon and have been identified previously to be $Fe_{25}Al_{60}Si_{15}$ for the intermediate layer, Fe_2Al_7Si for the plate-shaped phase, and $FeAl_4Si$ for the needle-shaped phase found in the matrix [7]. The intermediate layer and plate-shaped phases, which are close to the sphere walls, also contain small amounts of chromium and trace amounts of manganese.

The Vickers hardness value of the intermediate layer is highest in the air-cooled 740 °C sample (708.1 HV). Hardness of the intermediate layer in the air-cooled 700 °C sample was much lower at 572.1 HV, and the intermediate layer in the water-cooled 700 °C sample showed the lowest hardness at 553.9 HV. Hardness values of the plate-shaped phase show a similar trend, with 736.1 HV for the air-cooled 740 °C sample and 551.6 HV for the water-cooled 700 °C sample.

The monotonic compression results of water-cooled 700 °C, air-cooled 700 °C, and air-cooled 740 °C samples are presented in Fig. 5. All composite foam samples exhibit the typical metal foam behavior under compression including the linear elastic region, long plateau region, and densification region, although it should be noted that the energy absorption capability of all composite metal foams is much larger than that of other metal foams and bulk aluminum alloys [7, 19–21].

Fig. 2 Higher magnification SEM images of the sphere-matrix interface area taken at 100× magnification (**a**, **c**, **e**) and the boxed area enlarged to 450× magnification (**b**, **d**, **f**). Images (**a**) and (**b**) are from air-cooled 740 °C composite foam, Images (**c**) and (**d**) are from air-cooled 700 °C composite foam, and Images (**e**) and (**f**) are from water-cooled 700 °C composite foam

Discussion

Effect of processing parameters on microstructure

The differences in the size and the compositions of the various ternary phases in Al-steel composite foam produced by the three processing scenarios are due to the differences in their casting temperature and solidification rates. It is well known that a higher casting temperature will produce a slower solidification rate in cast materials, since more heat must be removed before the melt can begin to solidify [22]. Also, temperature measurements taken during processing of Al-steel composite foams show that the cooling rate for water-cooled 700 °C samples is about twice as fast as for air-cooled 700 °C samples.

The intermetallic phases in all cast Al-steel composite foam samples form while the foam remains at elevated temperatures immediately following casting as a result of inter-diffusion between iron, chromium, and manganese present in the steel sphere walls and the aluminum and silicon present in the matrix. Diffusion is affected by several factors, including concentrations of the species present, size and solubility of the atoms with respect to each other, and temperature. The diffusion coefficient, D, is a quantity that accounts for interactions between the host and solute atoms and is specific to a particular diffusion couple. The rate of diffusion is increased at higher temperatures because of the exponential dependence between diffusion coefficient and temperature as shown in Eq. 1.

$$D = D_0 e^{-Q/RT} \tag{1}$$

The diffusion coefficient (D) is determined from the material temperature in degrees Kelvin (T), activation energy required to move an atom from one lattice site to
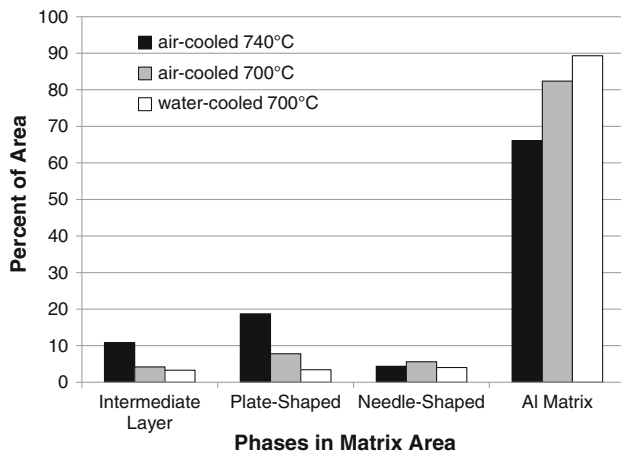
Fig. 3 Percentages of each phase present in the matrix area surrounding the hollow spheres using image analysis of the images shown in Fig. 1

Fig. 4 SEM images of needle-shaped phase morphology at 450× magnification in (**a**) air-cooled 740 °C composite foam, (**b**) air-cooled 700 °C composite foam, and (**c**) water-cooled 700 °C composite foam

another (*Q*), universal gas constant (*R*), and an additional temperature-independent constant specific to each diffusion couple (*D*$_0$) [23]. For iron atoms diffusing into aluminum, the diffusion coefficient spans several orders of magnitude in the temperature range present during cooling of the Al–steel composite foam. Similar behavior is observed for the diffusion of silicon into aluminum, with a three order of magnitude difference between diffusion coefficients at 700 °C and 500 °C. Table 2 shows values for diffusion coefficients of iron and silicon into aluminum reported in the literature at temperatures seen during cooling of Al–steel composite foam [24–26].

Consequently, the long exposure time to higher temperatures produced by a slow cooling rate or presence of a higher overheat allows the inter-diffusion of iron from the sphere walls and silicon and aluminum from the matrix to take place at a faster diffusion rate. As a result, the air-cooled 740 °C sample that experiences the slowest solidification rate and higher temperature exposure has the largest amount and size of intermetallic phases. In contrast, the air-cooled 700 °C sample has a smaller total percentage of intermetallic phases due to the faster solidification rate at the lower casting temperature. The water-cooled 700 °C sample shows further reduced size and total percentage of intermetallic phases through a combination of lower temperature exposure and the faster cooling rate obtained by the water-cooling method.

Intermetallic phases in the air-cooled 740 °C sample make up nearly 34% of the matrix area between the spheres, as opposed to about 18% for the air-cooled 700 °C sample and about 10% for the water-cooled 700 °C sample. The increased total percentage of intermetallics in slower cooling samples is largely due to the increased thickness of the intermediate layer and larger area and number of plate-shaped phases present (Fig. 1). It should be noted that the
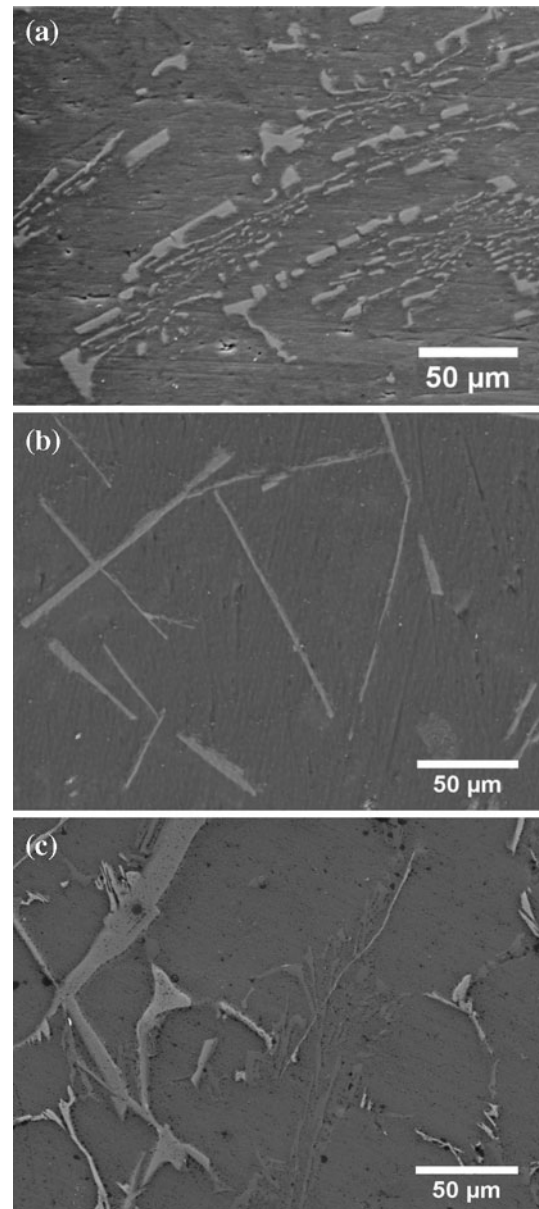
percentage of needle-shaped phases is largely unaffected by the diffusion of iron from the sphere walls since they are formed mostly by interaction between silicon and aluminum present in the matrix.

The pattern of intermetallic phase size and distribution for samples with each set of processing parameters is illustrated particularly well by the images of the sphere-matrix interface area shown in Fig. 2. The slow solidification rate of the air-cooled 740 °C sample allows time for the intermediate layer to grow thicker and also for iron atoms to travel far from the sphere walls into the matrix to form very large plate-shaped phases that have areas greater

Table 1 Elemental composition of the intermetallic phases in Al–stainless steel composite foams with various casting temperatures and cooling methods

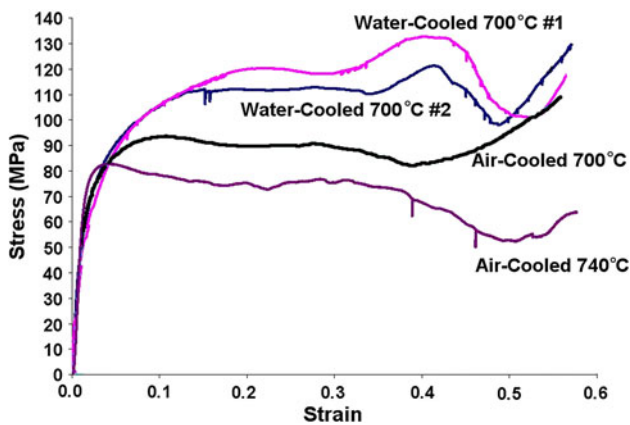|	Intermediate layer			Plate-shaped phase			Needle-shaped phase		
Casting temp. (°C)	740	700	700	740	700	700	740	700	700
Cooling method	Air	Air	Water	Air	Air	Water	Air	Air	Water
Al (at%)	72.17	71.1	73.54	72.46	73.61	73.04	82.48	70.11	67.45
Si (at%)	7.98	12.42	15.60	9.38	9.60	15.77	5.48	16.00	23.28
Fe (at%)	16.43	10.86	8.41	13.16	11.35	7.60	11.82	12.28	9.06
Cr (at%)	4.09	4.32	2.18	4.66	3.90	2.69	–	–	–
Mn (at%)	0.47	1.03	0.27	0.56	1.25	0.91	–	–	–

Fig. 5 Compression stress–strain curves of Al–stainless steel composite foams with various casting temperatures and cooling methods

Table 2 Diffusion coefficients of iron and silicon in aluminum at various temperatures

Temperature (°C)	$D_{Fe–Al}$ (cm²/s)	$D_{Si–Al}$ (cm²/s) [26]
500	1×10^{-12} [24]	1.28×10^{-9}
600	3×10^{-10} [24]	2.1×10^{-8}
700	4.5×10^{-8} [25]	1.0×10^{-7}
750	7.4×10^{-8} [25]	2.3×10^{-7}

than 30,000 μm². There are also a number of medium-sized (area between 6,000 and 20,000 μm²) and small (area <6,000 μm²) plate-shaped phases closer to the sphere walls that began forming at a later time than the large ones and would continue to grow as long as the foam is at high enough temperature for diffusion to take place.

The air-cooled 700 °C sample has about half as many plate-shaped phases, and all of these are in the medium-sized range of 6,000–20,000 μm². The intermediate layer of this sample is also much thinner. Since the solidification rate of this sample is faster, there is less time for elements to diffuse between the spheres and the matrix. As a result, the plate-shaped phases and intermediate layer are not able

to grow as large. It is also evident that the amount of diffusion is less by the lack of smaller plate-shaped phases forming close to the sphere walls as seen in the air-cooled 740 °C sample.

The effect of additional increase in cooling rate obtained in the water-cooled 700 °C sample is to further decrease the total area occupied by intermetallic phases. The fast cooling rate seen by these samples greatly restricts the ability of iron atoms to travel far from the sphere walls and resulted in more individual plate-shaped phases forming close to the sphere wall but with much smaller size (less than 3,000 μm²) than those seen in air-cooled 740 °C and air-cooled 700 °C samples.

The differences in composition and hardness values of the intermetallic phases produced in each sample are also explained by the rate of diffusion that is allowed. For the intermediate layer and the plate-shaped phases close to the sphere walls, as the solidification rate is faster, the percentage of aluminum stays about the same while the percentage of silicon increases and the percentage of iron decreases. This is a direct result of the ability of iron and silicon to diffuse between the spheres and the matrix to form intermetallics at higher temperatures as described by the diffusion coefficients in Table 2.

It should be noted that the diffusion coefficient of silicon in aluminum is significantly greater than that for iron in aluminum at any given temperature, with the difference more pronounced at lower temperatures. This behavior can be related to the sizes of the diffusing atoms relative to the aluminum matrix. The atomic radius of silicon (1.10 Å) is smaller than that of aluminum (1.25 Å) while the atomic radius of iron (1.40 Å) is larger than that of aluminum [27]. Consequently, more energy is required for the larger iron atoms to fit in an aluminum matrix. At high temperatures, all the atoms present have more mobility and it is equally easy for the aluminum to accommodate the larger-sized iron atoms or smaller silicon ones. At lower temperatures where atom mobility is decreased the diffusion of smaller silicon atoms is preferred. However, the total amount of diffusion is also affected by the concentration of species

present, and iron in the sphere walls has a much higher concentration than silicon in the matrix. This results in the total diffusion of iron being greater while the foam is at higher temperatures and total diffusion of silicon being greater while the foam is at lower temperatures. As a result, the air-cooled 740 °C sample with slow solidification rate has intermetallics with a greater percentage of iron than silicon, while in samples with faster solidification rates the intermetallics contain a higher percentage of silicon and less iron.

The high hardness values of the intermediate layer in the slow-solidifying air-cooled 740 °C sample is a result of the increased iron content of phases in this sample. As iron content in the intermediate layer is reduced in faster solidifying air-cooled 700 °C and water-cooled 700 °C samples, the hardness values of the intermediate layer also decrease.

The morphology and composition of the needle-shaped phases (shown in Fig. 4 and Table 1) are governed largely by the interaction between silicon and aluminum present in the matrix alloy. These phases do contain some iron, but the amount is fairly small since this phase is located far away from the sphere walls and it is not affected much by changes in the solidification rate. The aluminum and silicon content, however, follow opposite trends as the solidification rate of the sample increases. For the slow solidification rate seen in the air-cooled 740 °C sample, silicon that is initially precipitated in the needle-shaped phase has plenty of time to dissolve in the surrounding matrix at elevated temperatures. This results in needle-shaped phases with discontinuous, segmented morphology and low silicon and high aluminum contents. The air-cooled 700 °C sample solidifies somewhat faster and the result is thin, continuous needles with higher silicon and lower aluminum contents since the silicon has less time to dissolve in the matrix. For water-cooled 700 °C samples, the high solidification rate causes needle-shaped phases with a bulkier, more branched structure. Since silicon has very little time to dissolve in the matrix during water cooling, the needle-shaped phase in the water-cooled 700 °C sample has the highest silicon content and lowest aluminum content and remains in a shape close to how the phase was solidified.

Effect of processing parameters on mechanical properties

From the stress–strain curves shown in Fig. 5, it can be seen that mechanical properties of composite metal foams are controlled by both the casting temperature and the cooling method through their effect on the size and distribution of intermetallics formed at the interface of steel hollow spheres and aluminum matrix. Previous study has

shown that the hard and brittle intermetallic phases at the sphere-matrix interface can fracture under loading causing the spheres to de-bond from the matrix [7]. The fracture behavior of these hard intermetallic materials can be explained by Weibull fracture theory. The theory, widely applied to the fracture of ceramic materials, predicts that the brittle fracture strength of a hard material is a function of material size as well as the stress distribution [28]. Consequently, intermetallic phases of larger size, such as the large plate-shaped phases seen in the air-cooled 740 °C sample, are more likely to fracture under loading than smaller sized intermetallic phases in other samples.

When comparing the air-cooled samples cast at different temperatures, it can be seen that the amount of overheat in the melt significantly affects the properties of composite metal foam. The air-cooled 740 °C samples (20% overheat) exhibit the lowest strength. A close observation of the samples under loading showed that the deformation is less uniformly distributed through the sample and dominated by spheres de-bonding from the matrix. This is due to the presence of numerous large intermetallics formed at the sphere-matrix interface of these samples. In contrast, the deformation in the air-cooled 700 °C samples (15% overheat) was more uniformly distributed throughout the sample with the spheres and matrix remaining more intact under loading. These samples had a lower total percentage of intermetallics than air-cooled 740 °C samples and consequently showed higher plateau strength. From these results, it can be concluded that although 15–20% overheat is necessary to facilitate flow of molten aluminum around the hollow spheres during casting, stronger mechanical properties can be obtained with a 15% overheat rather than a 20% overheat.

The addition of water cooling resulted in higher strength and energy absorption when compared with the air-cooled samples. As shown in Fig. 5, the plateau strength of the water-cooled 700 °C samples is increased while maintaining densification strains comparable to air-cooled samples in the range of 55–60% strain. Such a combination of high plateau strength and large densification strain is required to maximize the material's energy absorption capability. The faster solidification rate seen by the water-cooled 700 °C samples reduces the size, total amount, and hardness of intermetallics that form in the composite metal foam microstructure. This results in water-cooled 700 °C samples showing the highest plateau strength and energy absorption out of all the samples tested.

The mechanical properties of cast Al–steel composite foam can be altered by controlling the amount of intermetallics present in the microstructure, which can be achieved by careful selection of processing parameters. An overheat of 15% in addition to a fast water-cooling technique will help to minimize intermetallic formation and

consequently achieve higher mechanical properties and energy absorption capability.

Conclusions

The microstructure and mechanical properties of cast Al–steel composite foam were examined for samples processed at casting temperatures with 15% overheat (700 °C) and 20% overheat (740 °C) in addition to both air and water cooling methods. Lower casting temperatures resulted in a faster solidification rate of the foam, and the addition of the water-cooling technique further increased the material's solidification rate. Processing parameters were found to affect the composite metal foam microstructure by altering the size, distribution, composition, and hardness of intermetallic phases present. A direct relation between the microstructure of the Al–steel composite foams and their mechanical properties was established, with the strength and energy absorption increasing as intermetallic content in the microstructure decreases. This reduction in the intermetallic phase content can be brought about by fast solidification that limits the diffusion of elements between the sphere walls and the matrix. It is also concluded that while a minimum overheat of 15% is necessary to obtain optimum fluidity of the melt while minimizing the formation of intermetallics at the interface of steel spheres and the aluminum matrix, the 20% overheat seemed to promote such intermetallic formation and lowered the mechanical properties of Al–steel composite foam. The highest strength and best energy absorption properties were obtained with the water-cooled samples cast at 700 °C resulting from an optimum overheat (15%) and solidification rate.

References

1. Ashby MF, Evans AG, Fleck NA, Gibson LJ, Hutchinson JW, Wadley HNG (2000) Metal foams: a design guide. Butterworth-Heinemann, Woburn, MA
2. Sugimura Y, Rabiei A, Evans AG, Harte AM, Fleck NA (1999) Mater Sci Eng A 269:38
3. Rabiei A, Vendra L, Reese N, Young N, Neville B (2006) Mater Trans 47:2148
4. Rabiei A, Neville B, Reese N, Vendra L (2007) Mater Sci Forum 539–543:1868
5. Rabiei A, Vendra L (2009) Mater Lett 63:533
6. Rabiei A, O'Neill AT (2005) Mater Sci Eng A 404:159
7. Vendra LJ, Rabiei A (2007) Mater Sci Eng A 465:59
8. Vendra L, Neville B, Rabiei A (2009) Mater Sci Eng A 517:146
9. Vendra L, Rabiei A (2010) Mater Sci Eng A 527:1784
10. Cheng HF, Han FS (2003) Scripta Mater 49:583
11. Gupta SP (2003) Mater Character 49:269
12. Viala JC, Peronnet M, Barbeau F, Bosselet F, Bouix J (2002) Composites A 33:1417
13. Maitra T, Gupta SP (2003) Mater Character 49:293
14. Villars P, Prince A, Okamoto H (1995) Handbook of ternary alloy phase diagrams. ASM International, Materials Park
15. Fragner W, Zberg B, Sonnleitner R, Uggowitzer PJ, Loffler JF (2006) Mater Sci Forum 519–521:1157
16. Kupp DM, Claar TD, Stephani G, Waag U (2001) In: Advances in powder metallurgy and particulate materials, Part 8: Refractory metals, carbides, cermets, ceramics, foams; May 13–17, p 1486
17. ASM Handbooks Online Volume 3 Alloy Phase Diagrams (2009) ASM International, Materials Park. http://products.asminternational.org/hbk/index.jsp. Accessed 18 Aug 2010
18. Li P, Nikitin VI, Kandalova EG, Nikitin KV (2002) Mater Sci Eng A 332:371
19. Olurin OB, Fleck NA, Ashby MF (2000) Mater Sci Eng A 291:136
20. Andrews E, Sanders W, Gibson LJ (1999) Mater Sci Eng A 270:113
21. Sugimura Y, Meyer J, He MY, Bart-Smith H, Grenstedt J, Evans AG (1997) Acta Mater 45:5245
22. Srinivasan A, Pillai UTS, Pai BC (2006) Int J Micro Mater Prop 1:139
23. Borg RJ, Dienes GJ (1988) An Introduction to Solid State Diffusion. Academic Press Inc, Boston
24. Mantl S, Petry W, Schroeder K, Vogl G (1983) Phys Rev B 27:5313
25. Xingqing W, Wood JV, Yongjiang S, Haibo L (1998) J Shanghai Univ 2:305
26. Fujikawa S, Hirano K, Fukushima Y (1978) Metall Mater Trans A 9:1811
27. Slater JC (1964) J Chem Phys 41:3199
28. Petrovic JJ (1987) Metall Mater Trans A 18:1829